NUMERICAL ANALYSIS ON FATIGUE LIFE PREDICTION OF CANCELLOUS BONE RESPECT TO NORMAL WALKING LOADING

Mohammad Mostakhdemin[1], Fatihhi S.J.[1], Muhamad Noor Harun[1,2], Ardiyansyah Syahrom[1,2*]

[1]Faculty of Mechanical Engineering,
Universiti Teknologi Malaysia,
81310 UTM Johor Bahru, Johor,
Malaysia

[2]Sport Innovation and Technology Centre,
Universiti Teknologi Malaysia,
81310 UTM Johor Bahru, Johor,
Malaysia

ABSTRACT

Osteoporosis disease makes bone fragile and weak to withstand against load and bodyweight. Damage initiated depends on different morphological indices and angle of oriented trabeculae. Fatigue analysis performed in strain-based approach for bovine trabecular bone in three different cases respects to its morphological indices to investigate correlation between fatigue life and bone morphology. On-axis and off-axis load effects are considered to determine trabecular yielding which is a main cause of failure. Once load impose as on-axis on trabecular, fatigue failure occur in high cycles (> 12226), however, off-axis load, which may impose on trabecular with 45 degree or perpendicularly cause drastically decrease of trabecular life. The most failure occurs in arc and rod-like trabecular and S-N curve for axial compression load were performed based on Coffin-Manson equation. Results had shown that with 20.2% loss of volume fraction (BV/TV) and 15.8% loss of surface density (BS/TV) fatigue life of trabecular bone by axial compression load decrease to 63.6%.

Keywords: *Fatigue, Cancellous bone, Trabecular bone, FE Simulation*

1.0   INTRODUCTION

Trabecular bone plays an important role in skeleton structures due to daily activities. Osteoporosis disease makes bone fragile more respect to healthy one and increase risk of fracture [1-3]. Since 70% of total load is tolerated by trabecular bone, this part of bone structure should be investigated in osteoporosis disease that bone involved [4]. Study of fatigue in bone has a contribution for designer of implants to find out about interaction between trabecular bone and prosthesis, recognizing weakens part of bone for treatment approach in drug-based delivery. Since there are fewer data in fatigue analysis of trabecular bone respect to the cortical one [5-8], this study focuses on fatigue part of trabecular structure taken from hip of bovine bone.

_____
*Corresponding author: ardi@mail.fkm.utm.my

The most portion of load imposed on hip is axial compression loading during daily activities. Multi axial stress is distributed over the bone due to tensile and compressive axial load [9]. Compression loading cause yield strain in on-axis loading, however, yield strain in off-axis increased and reduction in strength is greater than modulus [10]. In addition, some morphological indices are affected by osteoporosis disease that are known as volume fraction (BV/TV), surface density (BS/TS), trabecular number (Tb.N) and so on, which among of these parameters, BV/TV has an excellent correlation with yield strain and bone failure [11-13] and could be counted as a major parameter of failure of trabeculae within osteoporotic bone. Thus, axis of loading has a useful contribution on fatigue life of bone [14] Loss of volume fraction exceeds stress distribution all over the bone and within cyclic loading, damage initiation and crack growth occur in weaken trabeculae [1]. While cyclic load imposed on bone, modulus degradation and permanent strains were found in high stress tissues. Residual strain increased when compressive strain increase continuously to its maximum value [15]. Since post-test mechanical properties were most depends on maximum compressive strain and suggested that trabecular bone failure is largely strain based [16], thus, in this study strained-based approach was used to predict fatigue life of trabecular bone. On-axis and off-axis load was simulated to find out correlation of loading orientation angle on trabecular failure.

2.0   MATERIALS AND METHODS
2.1   Sample Preparation

Trabecular bone samples were extracted from hind limb of fresh bovine cadavers gathered from a local slaughterhouse. The trabecular bone samples were then cut from the femoral head using a ±150 rpm diamond saw (Behringer GmbH, typeSLB 230 DG HA, Kirchardt) under copious lubricant irrigation to minimize heat generation and strut breakage. Saline water was used as lubricant to ensure that the temperature did not exceed 46°C to protect the sample from heat-related damage [17]. An infrared thermometer (Fluke 62 Mini Infrared Thermometer) was used in order to observe the temperature of the samples based on the blade and coring bit. During the cutting and drilling procedure, the process was stopped at several stages to measure the temperature in order to not to exceed the critical level. Cylinder samples with a total length of 10 mm and a diameter of 8 mm were then drilled using a 1.5 mm thick diamond-tip coring bit at 150-250 rpm [18]. The cylindrical bone samples were then cleaned using an ultrasonic cleaner [18, 19] with a chemical detergent for 3 hour [20, 21]. Water jets and air jets were used to remove any excess of water, fat and bone marrow from the bone samples. The procedure was repeated until no bone marrow could be detected upon visual inspection [21, 22]. The bone samples were then dried using an air jet and stored in a freezer individually in an airtight plastic bag to minimise thermal cycling [23-26]. The temperature of the freezer was set to -20°C [20, 23-26].

2.2   3D Modelling

Specimens were scanned by sky scan 1172 (Kartuizersweg 3B, 2550 Kontich, Belgium) and computed tomography (CT) images of bovine bone were used to construct 3D dimensional model as our trabecular samples. The CT images captured from femoral head of bovine bone and with resolution of 17.2 μm was set up for model construction [27]. Semi-automatic segmentation approach was applied to construct trabecular bone models (Mimic software, Materialise, Belgium). The software marching cube algorithm was used to generate element and mesh for pre-processing part of finite element analysis. Figure 1 shows a trabecular sample constructed in the mimics software.

Figure 1: Trabecular bone model

Marching Cubes method (MCM) was used to calculate bone surface area (BS). In this method, surface has been triangulated and tetrahedrons technique was applied to calculate bone volume (BV). Total volume (TV) is the volume of whole bone structures. Calculated morphological indices tabulated in Table 1.

Samples	BV/TV	BS/TS
Horizontal	0.159	2.957
Vertical	0.199	3.5
Oblique	0.172	3.042

Table 1: Trabecular bone morphological indices

2.2 Samples Excised

Based on on-axis and off-axis load orientation angle, we extracted three models. Since test performed on femur bone which shown three oriented loads angle during physiological activities that imposing on hip as F_x, F_y and F_z , three angles ($0°, 45°, 90°$) were selected to impose load on trabecular models as shown in Figure 2.
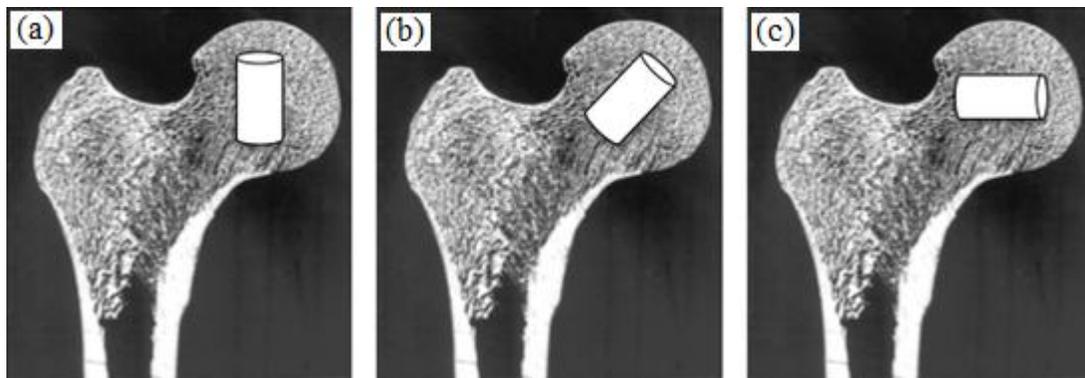
Figure 2: Trabecular samples prepared for simulation (a) vertical model (b) oblique model (c) horizontal model

2.2   Finite Element Simulation

Convergence study has been done, to finalize number of element for saving computational time as illustrated in Figure 3.
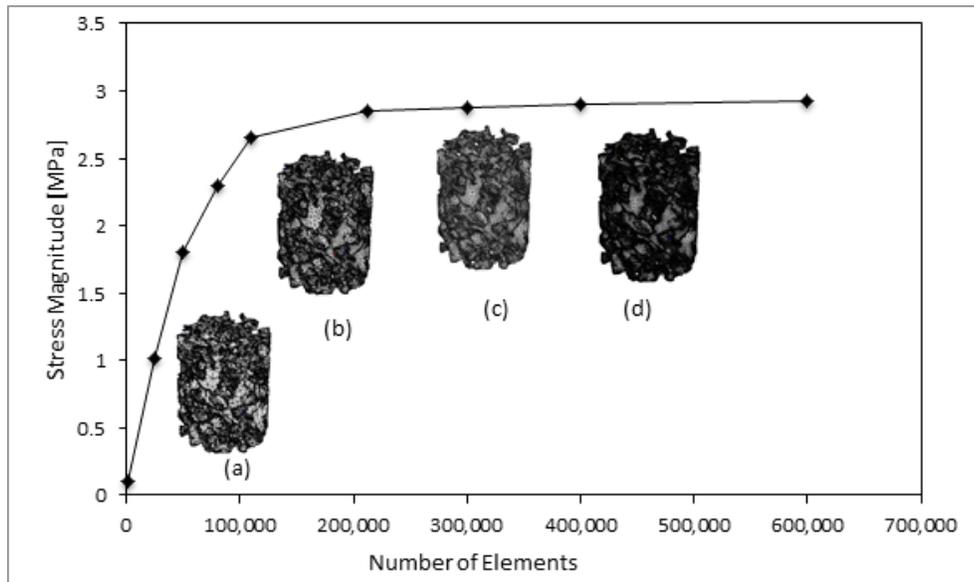
Figure 3: Mesh convergence study. Mesh (b) was selected for all models as has same results in stress magnitude, but lower computational time.

Beyond the mesh convergence study, mesh quality technique was used to check quality of mesh in finite element software COMSOL Multiphysic (COMSOL Multiphysic software version 4.3 b, Burlington, USA) to make sure about recognition of high quality of elements by finite element package that used for simulation. A tetrahedral element 4-node was selected and mesh quality check of vertical, oblique and horizontal model are shown as a sample in Figure 4. Red and blue elements are representative of high and low mesh quality respectively.
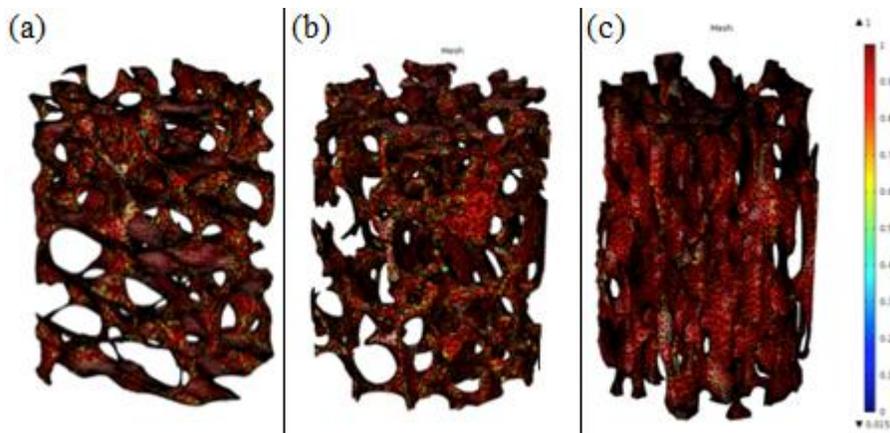
Figure 4: Mesh quality of (a) horizontal model (b) oblique model (c) vertical model

Samples imported into FE package software need to identify load and boundary conditions on structure. First set of analysis has been done for axial loading, fixation part of trabecular bone is as shown in Figure 5 lowest surfaces were fixed in all directions and for upper surfaces, distributed load was imposed for fixed part or fixed boundary.

Figure 5: Load and boundary on trabecular bone

The best-fit algorithm code was developed to extract polynomial coefficients through MATLAB software from the genuine graph of gait cycle trend is in body weight percentages. Polynomial equations in Fx, Fy and Fz which are shown in Appendix 1.

2.4   Tissue Properties Modelling

Trabecular bone of femur was modelled as linear isotropic behaviour with E = 18 MPa, ν = 0.3 [28] σ_y = 8.4 MPa [29]. Strain hardening model was developed for trabecular bone to describe yielding of trabecular bone at the continuum level. Kinematic tangent modulus for trabecular bone was defined 0.9 GPa. Strain-based method as fatigue model was selected which is combination of elastic part by Bassquin law and plastic part covered by Coffin-Manson law. Fatigue data parameter assigned as ductility coefficient $\varepsilon_f{'}$ = 0.352, fatigue ductility exponent b = -0.981, fatigue strength coefficient $\sigma_f{'}$ = 6 MPa, fatigue strength exponent c = -0.096 [30].

3.0   RESULTS AND DISCUSSION

Two different types of result are covered; first stress analysis of three samples in axial loading, then fatigue life prediction of trabecular bone will be represented. Finally, correlation among different samples with different morphological indices will be discussed. Maximum stress and effective plastic strain are covered as static analysis and stress versus number of cycles to failure in axial loading for three samples that called dynamic analysis. Among different bone morphology indices, volume fraction (BV/TV) and surface density (BS/BV) were selected as criteria of osteoporotic bone to find correlation of fatigue life of bone and morphological indices. Von-Mises criteria are used to track the stress distribution and amplitude. Effective plastic strain presents the best representative of damage initiation. Vertical model with less porosity than oblique and horizontal model is subjected to axial loading involving lower stress amplitude and effective plastic strain as well (average range 3.35 MPa) which is shown in Figure 6.
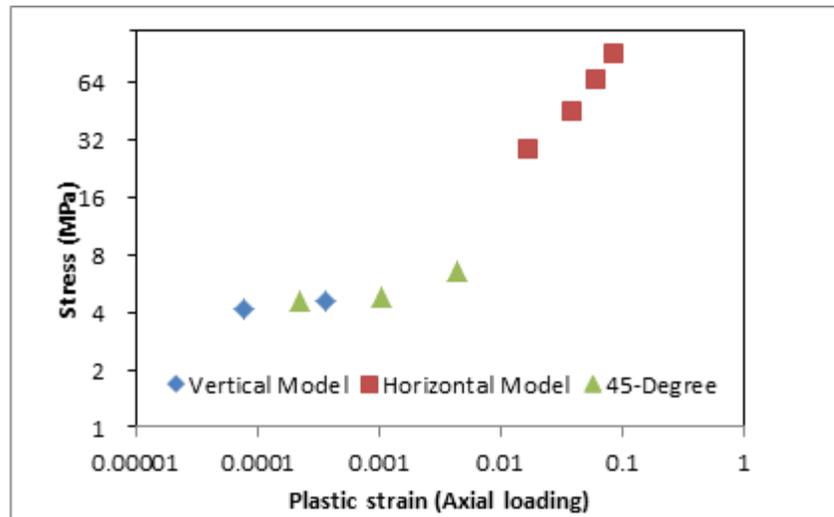
Figure 6: Stress-effective plastic strain of vertical model

Since the vertical model includes more plate-like trabecular, plastic strain is localized and initiated at 30% of load. Furthermore, 4.11 MPa is the stress value of this load percentage. Then with load increment, the plastic strain has no considerable increment. In addition stress localization is occurred in rod-like trabecular. In the range of 20%-30% of total load this trend increases considerably, however, in 30%-40% this trend increase slightly. Oblique model with more porosity than vertical and less than horizontal, took higher stress magnitude compare with vertical and lower stress amplitude than horizontal. Non-uniformity stress distributed over the structure in oblique model is as illustrated in Figure 7.
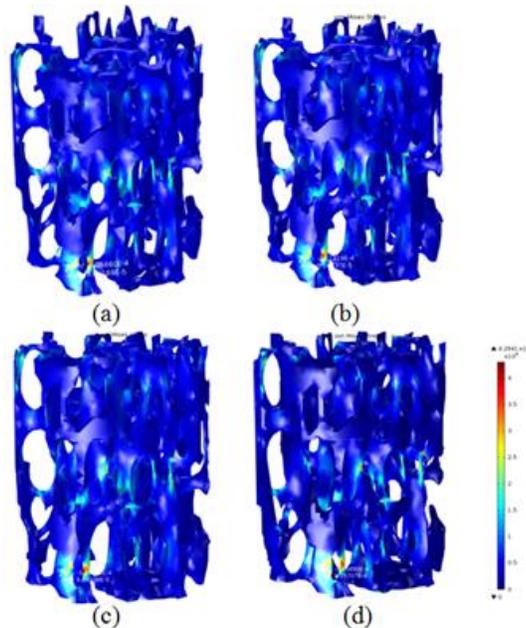
Figure 7: Stress analysis results of vertical model (a) 10% of total loading (b) 20% of total loading (c) 30% of total loading (d) 40% of total loading

Since porosity of oblique is more than vertical model so it is expected that plastic strain initiated in lower stress amplitude based on load percentage. In this part of analysis, with 20% of total load plastic strain initiated with 0.0002,however this value reach to 0.004 when structure is subjected to 6.61 MPa stress amplitude. In comparison with the vertical sample that stress amplitude was maximum in 40% of total load. The trend of stress versus effective plastic strain in the vertical model is increase sharply in 30% of total load, after that increase slowly until 40% of total load. However, in oblique this trend is completely different, from 10% to 20% there is sharp increase and then in the range of 20%-30% approximately constant that show with constant stress amplitude effective plastic strain increase considerably. The stress distributed over the structure in the 45-degree model is as illustrated in Figure 8.
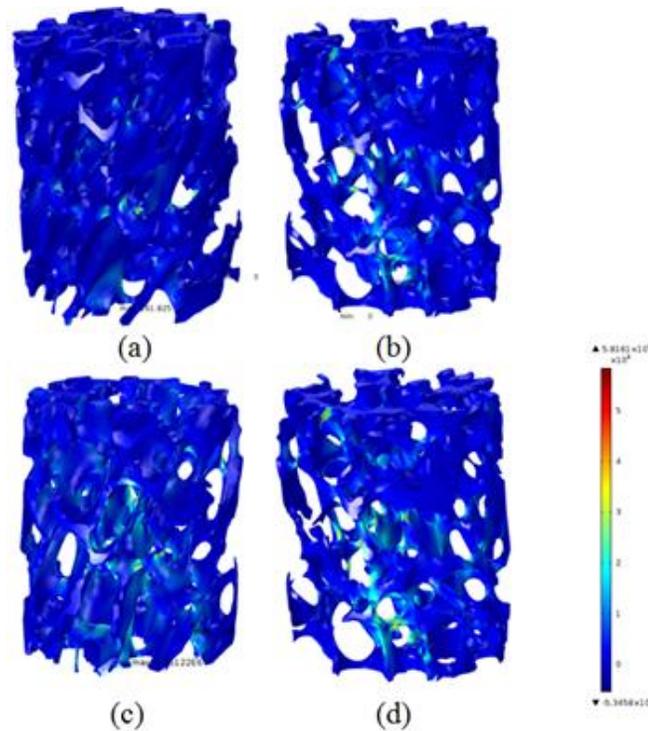
Figure 8: Stress analysis results of 45-degree model (a) 10% of total loading (b) 20% of total loading (c) 30% of total loading (d) 40% of total loading

Horizontal model with more porosity than oblique and vertical model subjected to axial loading is faced with higher stress amplitude and effective plastic strain as well. Here the trend of load percentage increment and its result are shown in Figure 9.
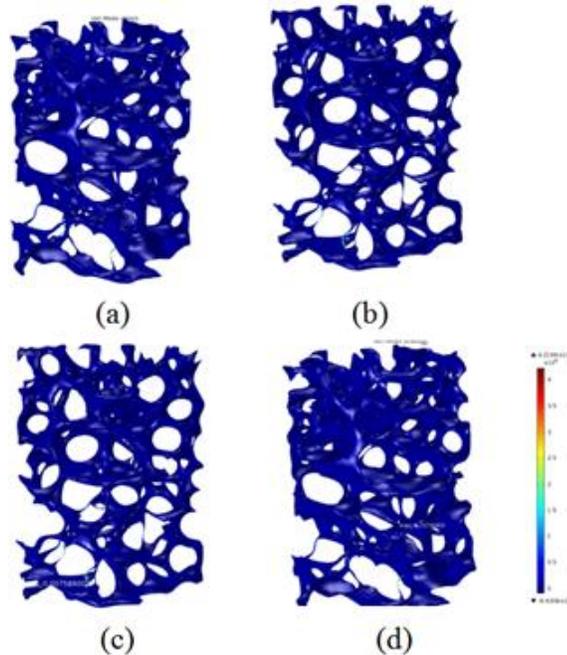
Figure 9: Stress analysis results of horizontal model (a) 10% of total loading (b) 20% of total loading (c) 30% of total loading (d) 40% of total loading

Horizontal model is simulated as worse case respect to osteoporotic bone; this model cannot withstand high stress amplitude and plastic strain as well. Plastic strain initiated at first 10% of total loading with 90.7 MPa stress amplitude and 0.086 effective plastic strain, in compare to the previous models (vertical and oblique), stress amplitude increase considerably and larger amount of plastic strain at load amplitude did some damage to weakest rod-like trabeculae. As is clear from Figure 6, stress increase till 30% of total load that is not too much increased value respect to the 10% and 20%, however, in 40% of total load this value increase sharply to 716 MPa and 0.211 as effective plastic strain. In comparison with the oblique sample that increase till 6.61 MPa as stress amplitude. In dynamic analysis, fatigue life estimation was aimed. Since strain-based method was applied as fatigue model, so strain amplitude versus number of cycles to failure was plotted for three samples. Since vertical model is less porosity than two other samples, it would be expected that fatigue life of vertical model is longer than other two samples. Here fatigue analysis result of trabecular bone and its S-N curves are presented in Figures 10 and 11 while the plots of the vertical model are presented in Figures 12 and 13.
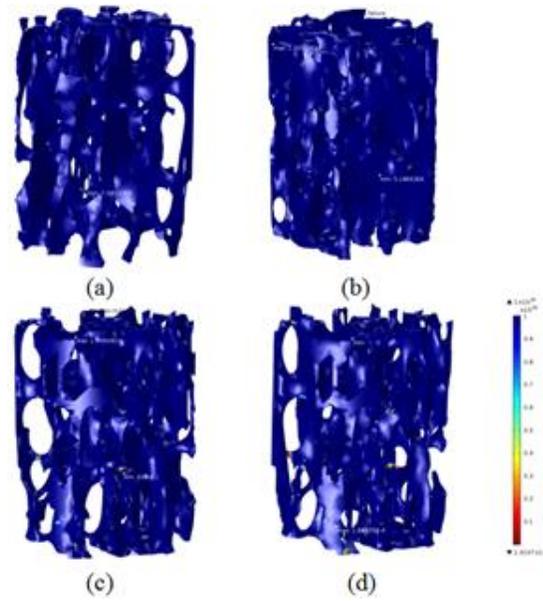
Figure 10: Number of cycles to failure of vertical model (a) 10% of total loading (b) 20% of total loading (c) 30% of total loading (d) 40% of total loading

$$y = -9E\text{-}15x + 9E\text{-}05$$
$$R^2 = 0.59063$$
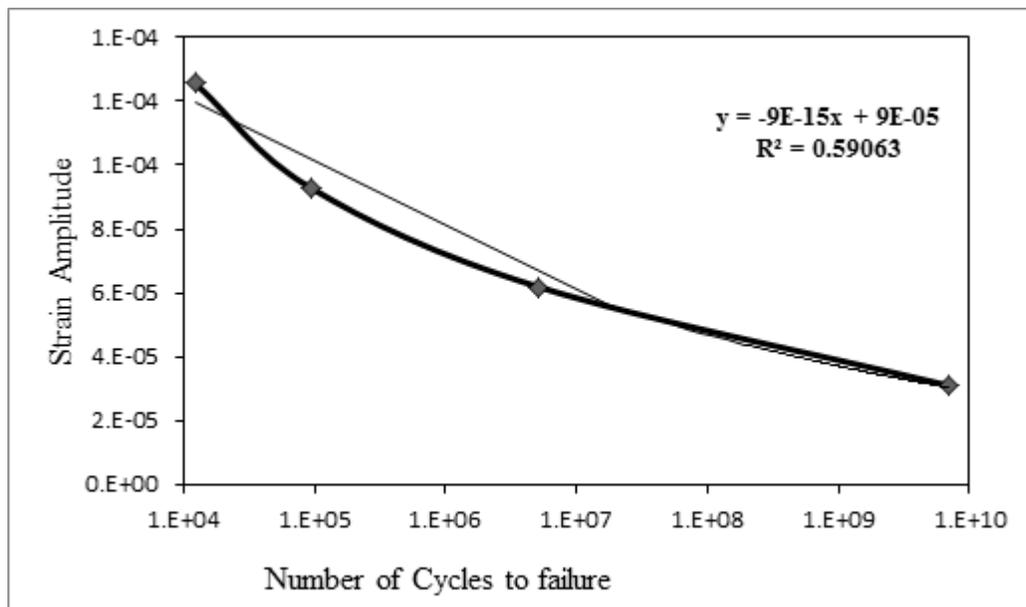
Figure 11: S-N curve for vertical model
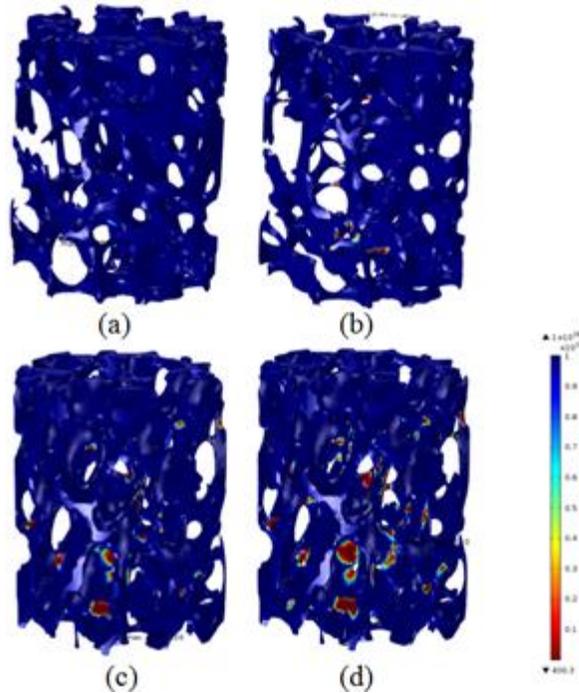
Figure 12: Number of cycles to failure of oblique model (a) 10% of total loading (b) 20% of total loading (c) 30% of total loading (d) 40% of total loading.

$$y = -4E-10x + 0.0003$$
$$R^2 = 0.64411$$
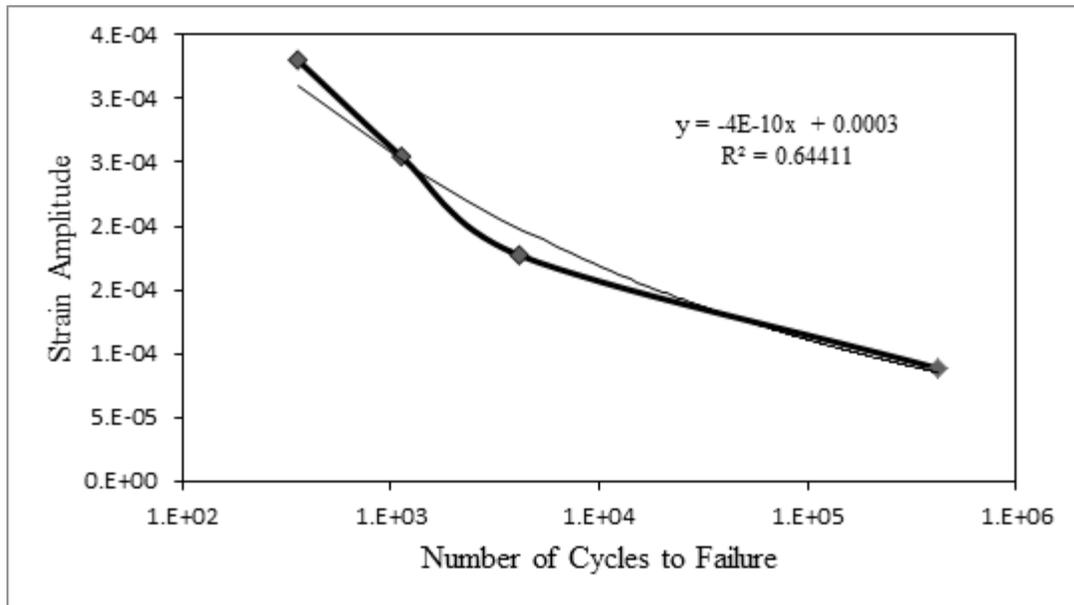
Figure 13: S-N curve of 45-degree

Since the oblique sample porosity is more than vertical model and number of its rod-like is more than rod-like in vertical sample, fatigue life prediction in this sample decrease respect to the vertical one. In 10% of total load, fatigue life is 4e5 cycles to failure and in 40% this value decrease drastically to 357 cycles that in comparison with vertical model in 40% of total load is counted 2.9% of its life. As is clear in Figure 12, stress localization is initiated in the arch and growth by

increasing load amplitude. Meanwhile trabecular bone study play an important role due to its correlation with osteoporosis disease and its morphology, so analysis of trabecular bone in the sense osteoporotic bone makes a useful contribution. Thus, Figure 14 showed the behaviour of osteoporotic bone under axial compression load and S-N curve for the horizontal model is presented in Figure 15.
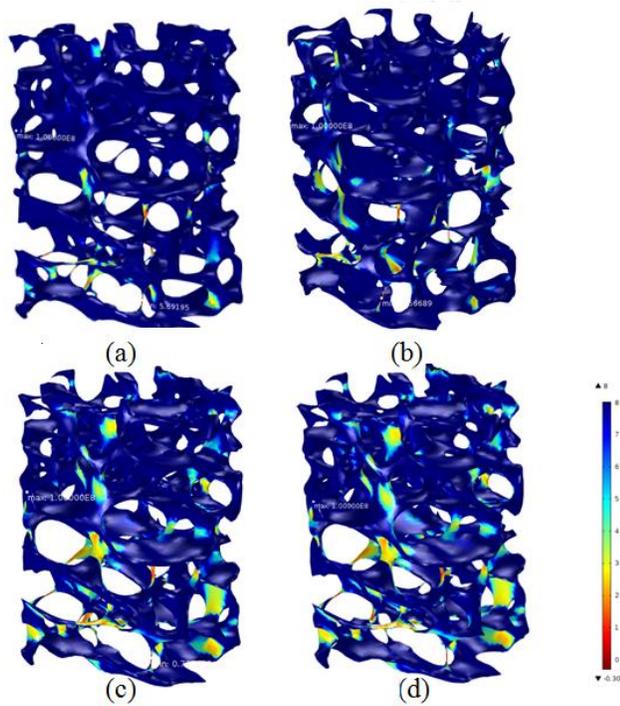
Figure 14: Number of cycles to failure of horizontal model (a) 10% of total loading (b) 20% of total loading (c) 30% of total loading (d) 40% of total loading

$$y = 0.0387x^{-0.564}$$
$$R^2 = 0.998$$
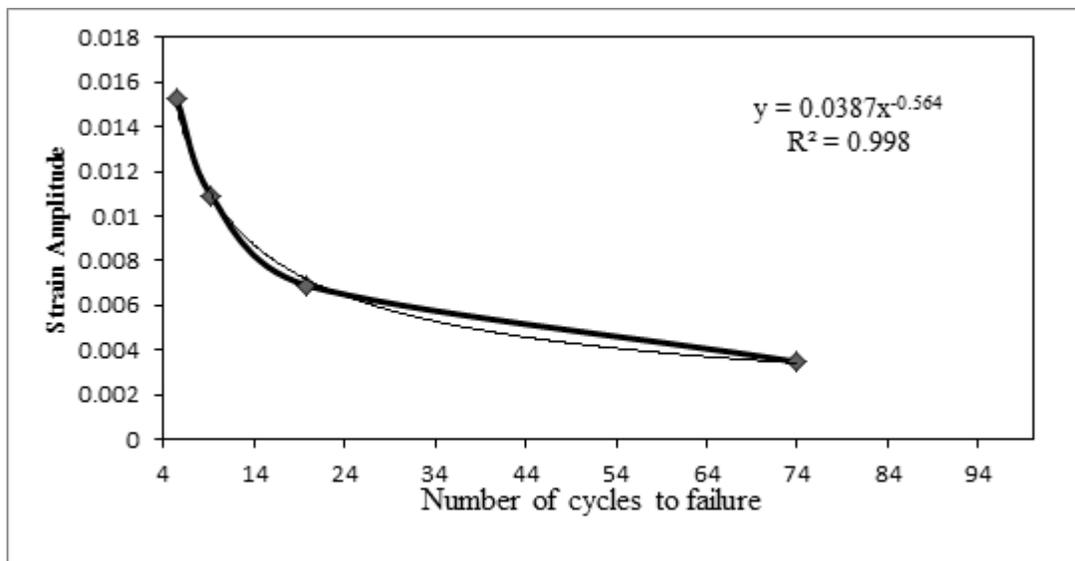
Figure 15: S-N curve of horizontal model

Horizontal model was included many weak rod-like trabeculae that make structure fragile and fatigue life decrease drastically. In the horizontal sample, with 10% of total load fatigue life of trabecular bone is 73 cycles and at 40% of total load it will reach to 5 cycles. In comparison to the oblique and vertical samples 40% of total load decrease drastically to small amount of value and diminish of rod-like and plate-like of trabecular bone has functionality with the failure within structure.

4.0 DISCUSSION

Osteoporosis disease makes bone fragile and cause bone has shorter life that close to fracture in low number of cycles due to physiological activities. Fatigue life of trabecular bone is depend on various parameters; different type of load imposed on it, morphological indices such as BV/TV, BS/TS, in different anatomical sites, load and its direction that makes it close to fatigue life or damage in inner site.

In this analysis fatigue applying strain-based method, results shown that fatigue is altered based on morphology indices and porosity that is different within anatomical sites performed life estimation. Vertical model that was counted as vertical specimens taken from femoral head was withstood of load more than other two samples. This reason is because of its porosity that makes it strong enough. Plastic strain is initiated at 30% of total load. However, in oblique and horizontal model yield stress initiated at 20% and 10% of total load respectively, that shown with more porosity, plastic strain decrease drastically and this functionality can be considered as one of the crucial factor in bone fracture.

In dynamic analysis, the S-N curve extracted and results show that trabecular bone follow the Coffin-Manson law and considered as a reliable method for estimation of fatigue life of the trabecular bone. In such analysis, the life of trabecular bone will decrease by increasing the load amplitude and plastic strain initiated and growth in arch of rod-like of trabecular. Vertical sample had longer life respect to the other two samples and results shown that most fracture occur when load angle is perpendicular with trabeculae. Number of cycles to failure has functionality with porosity and trabeculae orientation angle. While load impose by 45 degree to the trabeculae, rod-like failed at 20% of total load. Rod-like can tolerate when load impose on it as on-axis of trabecular direction.

5.0 CONCLUSION

As a results obtained in this study and some literature that have carried out by other researchers, fatigue life estimation of trabecular bone is accurate in real bone that faced with osteoporosis disease and some cells in bone such as osteoblast and osteoclast has no ability to model and re-model bone with which this bone is counted as dead structure. For live bone and estimation of fatigue life, considering model and remodel of bone after every load cycles is highly recommended for further study. Also analysis of different types of load such as axial, torsional and multi-axial load and developing of models, which can predict fatigue life will be expected for those, are interested in such area.

REFERENCES

1. Burr, D.B., et al. (1997). Bone Microdamage and Skeletal Fragility in Osteoporotic and Stress Fractures. *Journal of Bone and Mineral Research*, 12(1), 6-15.
2. Muir, P., K.A. Johnson, and C.P. Ruaux-Mason (1999). In vivo matrix microdamage in a naturally occurring canine fatigue fracture. *Bone*. 25(5), 571-576.
3. Schaffler, M.B., K. Choi, and C. Milgrom, (1995). Aging and matrix microdamage accumulation in human compact bone. *Bone*. 17(6), 521-525.
4. Dendorfer, S., H.J. Maier, and J. Hammer. (2009). Fatigue damage in cancellous bone: an experimental approach from continuum to micro scale. *J Mech Behav Biomed Mater*, 2(1), 113-9.
5. Carter, D.R. (1981). Uniaxial fatigue of human cortical bone. The influence of tissue physical characteristics. *Journal of Biomechanics*, 14(7), 461-470.
6. George, W.T. and D. Vashishth (2006). Susceptibility of aging human bone to mixed-mode fracture increases bone fragility. *Bone*, 38(1), 105-111.
7. O'Brien, F.J., D. Taylor, and T.C. Lee (2003). Microcrack accumulation at different intervals during fatigue testing of compact bone. *Journal of Biomechanics*, 36(7), 973-980.
8. Yeni, Y.N., et al., (2009). Human cancellous bone from T12-L1 vertebrae has unique microstructural and trabecular shear stress properties. *Bone*, 44(1), 130-6.
9. Moore, T.L.A., F.J. O'Brien, and L.J. Gibson (2004). Creep Does Not Contribute to Fatigue in Bovine Trabecular Bone. *Journal of Biomechanical Engineering*, 126(3), 321-329.
10. Bevill, G., F. Farhamand, and T.M. Keaveny, (2009). Heterogeneity of yield strain in low-density versus high-density human trabecular bone. *Journal of Biomechanics*, 42(13), 2165-2170.
11. Hulme, P.A., S.K. Boyd, and S.J. Ferguson, (2007). Regional variation in vertebral bone morphology and its contribution to vertebral fracture strength. *Bone*, 2007. 41(6), 946-957.
12. Bevill, G., et al., (2006). Influence of bone volume fraction and architecture on computed large-deformation failure mechanisms in human trabecular bone. *Bone*, 39(6), 1218-1225.
13. Nazarian, A., et al., (2006). The interaction of microstructure and volume fraction in predicting failure in cancellous bone. *Bone*, 39(6), 1196-1202.
14. Dendorfer, S., H.J. Maier, and J. Hammer, (2009). Fatigue damage in cancellous bone: An experimental approach from continuum to micro scale. *Journal of the Mechanical Behavior of Biomedical Materials*, 2(1), 113-119.
15. Taylor, M., J. Cotton, and P. Zioupos, (2002). Finite Element Simulation of the Fatigue Behaviour of Cancellous Bone. *Meccanica*, 37(4-5), 419-429.
16. Moore, T.L.A. and L.J. Gibson, (2004). Fatigue of Bovine Trabecular Bone. *Journal of Biomechanical Engineering*, 125(6), 761-768.
17. Gronkiewicz, K., et al., (2009). Experimental research on the possibilities of maintaining thermal conditions within the limits of the physiological conditions during intraoral preparation of dental implants. *Journal of Physiology and Pharmacology*, 60 (8), 123-7.
18. Shim, V.P.W., et al., (2005). Characterisation of the dynamic compressive mechanical properties of cancellous bone from the human cervical spine. *International Journal of Impact Engineering*, 32(1-4), 525-540.
19. Grimm, M.J. and J.L. Williams, (1997). Measurements of permeability in human calcaneal trabecular bone. *Journal of Biomechanics*, 30(7), 743-745.
20. Kohles, S.S., et al., (2001). Direct perfusion measurements of cancellous bone anisotropic permeability. *Journal of Biomechanics*, 34(9), 1197-1202.

21. Nauman, E.A., K.E. Fong, and T.M. Keaveny, (1999). Dependence of Intertrabecular Permeability on Flow Direction and Anatomic Site. *Annals of Biomedical Engineering*, 27(4), 517-524.
22. Baroud, G., et al., (2004). Experimental and theoretical investigation of directional permeability of human vertebral cancellous bone for cement infiltration. *Journal of Biomechanics*, 37(2), 189-196.
23. Rapillard, L., M. Charlebois, and P.K. Zysset, (2006). Compressive fatigue behavior of human vertebral trabecular bone. *Journal of Biomechanics*, 39(11), 2133-2139.
24. van Lenthe, G.H., M. Stauber, and R. Müller, (2006). Specimen-specific beam models for fast and accurate prediction of human trabecular bone mechanical properties. *Bone*, 39(6), 1182-1189.
25. Teo, J.C.M., et al., (2007). Correlation of cancellous bone microarchitectural parameters from microCT to CT number and bone mechanical properties. *Materials Science and Engineering: C*, 27(2), 333-339.
26. Burgers, T.A., et al., (2008). Compressive properties of trabecular bone in the distal femur. *Journal of Biomechanic*s, 41(5): p. 1077-1085.
27. Bajuri, M., et al., (2013). Biomechanical analysis of the wrist arthroplasty in rheumatoid arthritis: a finite element analysis. *Medical & biological engineering & computing*, 51(1-2), 175-186.
28. Bayraktar, H.H., et al., (2004). Comparison of the elastic and yield properties of human femoral trabecular and cortical bone tissue. *Journal of Biomechanics*, 37(1), 27-35.
29. Zhou, B., et al., (2014). Dependence of mechanical properties of trabecular bone on plate–rod microstructure determined by individual trabecula segmentation (ITS). *Journal of Biomechanics*, 47(3), 702-708.
30. Dendorfer, S., et al., (2008). Anisotropy of the fatigue behaviour of cancellous bone. *Journal of Biomechanics*, 41(3), 636-641.

Appendix 1

The yielded polynomial equations (A1 - A3) based on 60 kg of body weight during normal walking extracted from gait loading graph with the best curve-fit algorithm are shown as follows:

$$F_x = 1e^6(-0.3091\,t^7 + 1.058\,t^6 - 1.41t^5 + 0.9215\,t^4 - 0.3032\,t^3 + 0.0441\,t^2 - 0.0012t + 0.0002)$$
(A1)

$$F_y = 1e^5(-0.9961\,t^7 + 3.4936\,t^6 - 4.4099\,t^5 + 2.181\,t^4 - 0.0717\,t^3 - 0.2461\,t^2 + 0.0488t - 0.0009)$$
(A2)

$$F_z = 1e^5(-2.6105\,t^7 + 6.3501\,t^6 - 3.2159\,t^5 - 3.2341\,t^4 + 3.9678\,t^3 - 1.4579\,t^2 + 0.202t - 0.0043)$$
(A3)